17th Australasian Fluid Mechanics Conference
Auckland, New Zealand
5-9 December 2010

Numerical Comparison of Air Flow Patterns in the Upper Airways of Adults and Neonates

N. M. Stringer[1], J. E. Cater[1], J. Eaton-Evans[2] and C. White[2]

[1]Department of Engineering Science
The University of Auckland, Auckland 1010, New Zealand

[2]Fisher and Paykel Healthcare Limited
15 Maurice Paykel Place, Auckland 2013, New Zealand

Abstract

Computational fluid dynamics was used to model air flow through the upper airways of an adult and a neonate. Geometries of the airways were obtained from CT scans and imported into ANSYS ICEM [1] for meshing. Meshes with 600,000 nodes for the adult model and 800,000 nodes for the infant model were generated. Boundary conditions were applied using flow rates of 32l/min for adult expiration, 22l/min for adult inspiration, 4.3l/min for neonate expiration and 6.5l/min for neonate expiration. There was good agreement between modelled velocities in the adult model with experimental particle image velocimetry measurements. The bulk of the airflow occured in the inferior and medial passages of the airways in the adult, and flow vorticity was present only internally along the solid boundaries. In the neonate model, a flow separation at the nasal valve caused recirculation and high vorticity in the centre of the flow. Larger pressure differences were measured across the neonate airways compared to the adult, due to the higher airway resistance to flow.

Introduction

The human respiratory system relies on inhalation and exhalation of air through the upper airway, comprised of the mouth and nasal passages in parallel. The main physiological functions of these airways are for olfaction and conditioning of the inspired air, involving warming, humidification and filtration, to protect the lungs [9]. Inhaled air entering through the nares divides into different channels, as shown in Figure 1. High speed flow occurs in the middle and inferior meatuses, while slow speed flow occurs in the narrow superior olfactory regions [6]. The anatomy of the neonatal airways is not simply a scaled down version of the adult airway [5]. The upper airways in infants resembles more of a tube that has less branching compared to the adult, reflecting the under-development of the anatomy. Since the infant tongue normally blocks the oral cavity during normal breathing, most of respiration is entirely nasal [7].

Previous studies have attempted to model airway flow through the nasal cavity using steady-state CFD. Ishikawa *et al.* [4] attemped to investigate unsteady flow in the airway during natural breathing. The work assumed air to be a Newtonian fluid, homogeneous and incompressible. A zero pressure boundary condition was placed at the trachea, while a uniform velocity field was specified at the nares. This approach has the drawback of over-simplifying the velocity pattern at the nares, which is unknown. Taylor *et al.* [12] approached this problem by incorporating the geometry of the external nose into their model. Solutions were compared between a model where boundary conditions were applied at the nares, and a model which which incorporated the external nose geometry, and significant differences were found between the velocity fields that were produced. This study emphasised the importance of including the external nose geometry in the airway models.

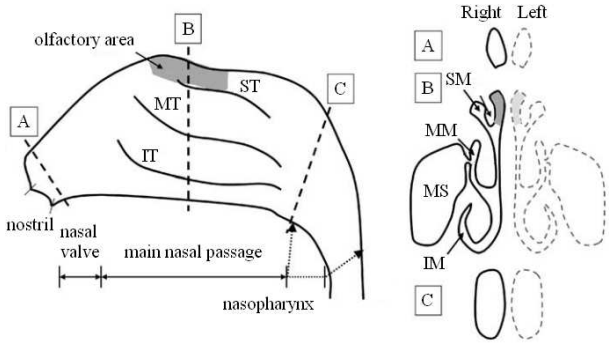

Figure 1: Schematic showing the anatomy of the nasal airway in one lateral plane and cross sections at A, B and C. IT, MT and ST correspond to the inferior, middle and superior turbinates while IM, MM and SM refer to the inferior, middle and superior meatuses. MS corresponds to the maxillary sinus. The olfactory region, shown in the superior air passage, is highlighted. Figure modified from [2].

Air flow velocity distributions during normal breathing have also been investigated *in vitro* using PIV [11]. Plastinated models were reconstructed from CT scans of adult airways and Reynolds number matched. These experimental results can be used to verify computational models. Croce *et al.* [2] used flow rates of up to 90l/s of three different gases to measure pressures *in vitro* to validate CFD models.

The aim of this project is to compare the flow through the upper airways of the adults and neonates using a CFD approach with physiologically appropriate boundary conditions. Results obtained computationally can then be compared with PIV results obtained by Spence *et al.* [11] which used the same geometric models and boundary conditions. Previous neonate models have not had sufficient geometric and spatial resolution for accurate modelling using CFD [7]. The objective is to form robust models that explain patterns of air flow in adults and neonates.

Turbulence Modelling

The Navier-Stokes equations, combined with the continuity equation, produce transient solutions for turbulent flows which are computationally expensive to compute. The equations can be time-averaged to produce the Reynolds Averaged Navier Stokes (RANS) equations (1), which are averaged over time [13]. This process divides the flow variables into a mean, time-averaged component and a fluctuating component.

$$\rho\frac{\partial \overline{u}_j\overline{u}_i}{\partial x_j} = \frac{\partial}{\partial x_j}\left[-\overline{p}\delta_{ij} + \mu\left(\frac{\partial \overline{u}_i}{\partial x_j} + \frac{\partial \overline{u}_j}{\partial x_i}\right) - \rho\overline{u_i'u_j'}\right] \quad (1)$$

The standard $k-\omega$ turbulence model was used to close these equations. This model has been found to be a better predictor of wall static pressures in the airway geometry over other RANS-type turbulence models [10].

Methodology

Domain

The airways geometry of the adult was taken from a healthy 44 year old male with the mouth closed using a medical CT scanner with 0.6mm spaced slices [11]. The neonate model was taken from a 42 week gestational age infant with 0.75mm slices using a CT scanner. The infant scan had an oral tube which did not affect the final geometry. These scans were segmented and imported into ANSYS ICEM [1]. Modifications to these geometries were required, including removal of artefacts from the scan, removal of the feeding tube in the infant, smoothing of the surfaces and closing of holes. The airway was assumed to be rigid, and the effects of the mucosal layer were ignored. The fluid used for computation was an ideal gas with a density of 1.068 kg m^{-3} and a dynamic viscosity of 1.88×10^{-7} kg m^{-1} s^{-1}. The temperature of the fluid was set to be 37°C. Due to the low velocities that develop throughout the airway relative to the speed of sound, the fluid can be regarded as incompressible [4].

An expanded rectangular domain was placed around the nose to specify an atmospheric boundary condition, so that the external nasal geometry could be taken into account. This appended domain was large enough to capture the region of high speed flow during expiration, but was not so large as to be computationally expensive. An artificial trachea pipe with a diameter to length ratio of 1:10 was also placed on the inferior end. The trachea of the neonate model had to be truncated closer to the nasopharynx compared to the adult model, which was necessary to close the oral cavity. These alterations allowed a more realistic boundary velocity profile to be generated at each end of the airway.

Boundary Conditions and Mesh Generation

Spence *et al.* [11] measured flow rates of 32l/min and 22l/min for peak expiration and inspiration flows, respectively, in the adult using a flow meter attached to a facemask, and calculated Reynolds numbers of 2225 and 1530 using PIV. These flow rates were specified as boundary conditions for the adult model. Flow rates of 4.3l/min and 6.5l/min for peak expiration and inspiration flows, respectively, in the neonate were calculated from average values of minute ventilation, respiratory rate and inspiratory/expiratory time constants [3]. These flow rates were used to calculate the normal velocity boundary across the tracheal end of the upper airway. A zero pressure atmospheric boundary condition was used on the surface of the exterior domain surrounding the nose.

The mesh was generated by first creating a coarse triangular surface mesh then a tetrahedral volume mesh. A global scale factor was reduced to produce finer meshes until the location of the maximum residuals and relative error of the solution were unaffected by further refinement. The mesh was generated in a similar manner for the infant model. It was deduced that 600,000 nodes (adult) and 800,000 nodes (infant) produced the optimal mesh size that modelled the flow without unnecessary computational expense. Due to the high flow gradients at no-slip boundaries, seven inflation layers were used with a growth ratio of 1.2, based from the size of the surface mesh. The mesh for the adult airway is shown in Figure 2; the infant mesh represented the geometry to a similar level of refinement.

Results and Discussion

Figures 3 and 4 show the air speed profiles for the adult and neonate models. In the adult, relatively high speeds are developed in the middle meatus during inspiration compared to the superior or inferior meatuses, in agreement with the experimental results using the same model [11]. Flow separation occurs as the incoming air divides into the different passages. During expiration, a high speed jet of air from the lower airway enters the superior part of the airway and high flow rates of 3-4m s^{-1}develop through both the superior and middle meatuses. The highest speeds occured through the nasopharyngeal section and through the nasal valve, due to the smaller cross-sectional areas in these sections. In contrast, flow patterns through the neonatal airway are different from those of adults. In this model, the turbinates have not fully grown and the bulk of the flow occurs through a main central passage. The length scale of the neonate model is approximately half the adult model. Much more activity can be seen in the nasal valve region during inspiration and expiration, where the large cavity suddenly narrows to form the nasal valve. The highest speeds also occur in the nasal valve, where the airway diameter is smallest. At the nasopharynx, different flow patterns are generated due to the difference in the way the trachea was modelled. In the adult, the expired air is pushed in an anterior direction while the jet is more dispersed in the neonate model.

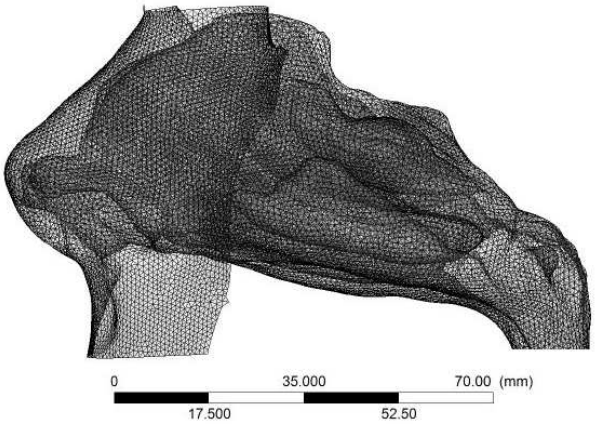

Figure 2: The surface mesh of the adult airway with 600,000 nodes. Not shown are the surface meshes for the external domains used to generate boundary conditions, or the trachea. Created with ANSYS ICEM [1].

Figures 6 and 7 show the non-dimensional vorticity magnitude profiles through the airway of the adult and neonate, as defined by equation 2:

$$\omega^* = \frac{\omega D_H}{U_{ave}} \tag{2}$$

where ω is the dimensional vorticity, D_H is the hydraulic diameter at the nasopharynx, and U_{ave} is the average air speed in the nasopharynx. The vorticity is a measure of the local rotation of the fluid. Vorticity is generated where the velocity gradients are high, which predominantly occurs at the fluid-solid boundaries in the adult model. This indicates that there is little rotation in the flow. However, large magnitudes of vorticities are generated in the nasal valve area of the neonate, which suggests that the geometry is causing the air to recirculate in this cavity. This recirculation acts as a region of large pressure change for air flowing into the airway during inspiration.

The pressures at the nasopharynx during the breathing cycle are shown in Figure 5. This was measured as an average pressure over a cross-sectional slice through the nasopharynx. The pressures developed by the adult agree well with data obtained by Croce et al. [2]. The neonate model experienced greater pressure differences between the atmosphere and the nasopharynx than the adult. The airway resistance can be quantified by the

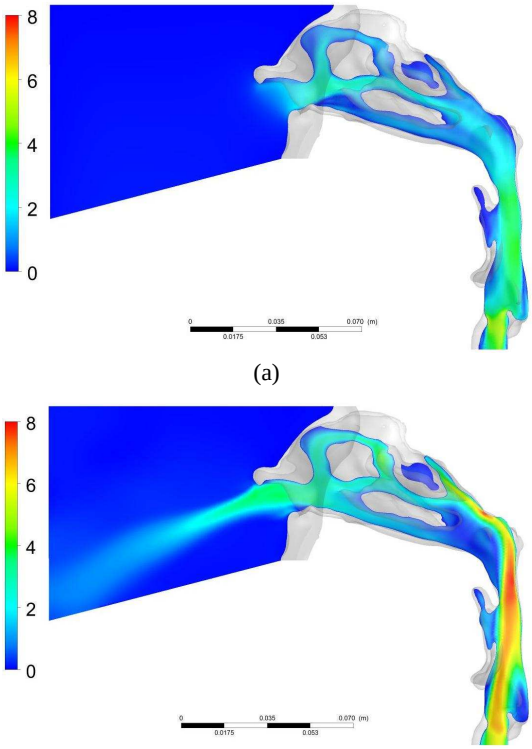

(a)

(b)

Figure 3: Air speed profile through a sagittal slice of the adult airway, during (a) inspiration and (b) expiration, in m s^{-1}.

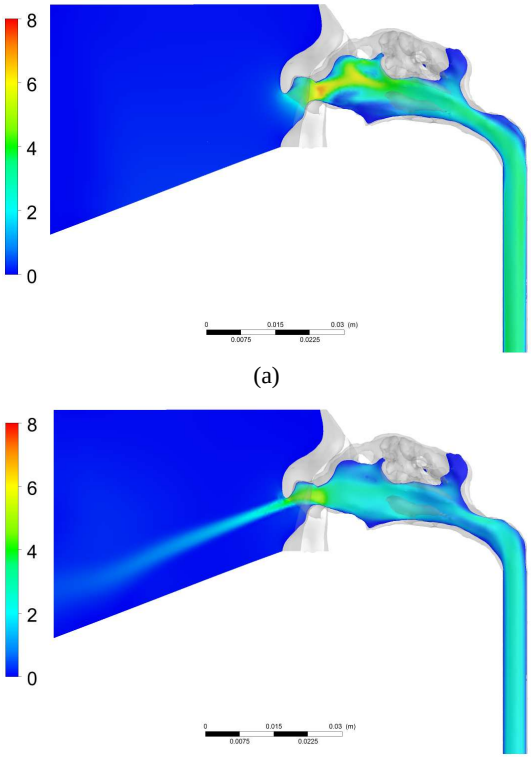

(a)

(b)

Figure 4: Air speed profile through a sagittal slice of the neonate airway, during (a) inspiration and (b) expiration, in m s^{-1}.

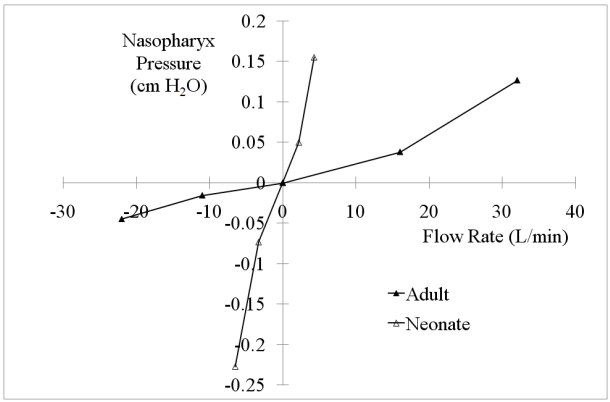

Figure 5: Pressure at the nasopharynx during the phases of breathing, for the adult and neonate models. Note that positive flow represents expiration. The pressures are measured relative to zero atmospheric pressure.

Darcy friction factor [8], given by equation 3:

$$f = \frac{p}{\frac{1}{2}\rho U_{ave}^2}\frac{D_H}{L} \tag{3}$$

where p, D_H and U_{ave} are the pressure, hydraulic diameter and average air speed at the nasopharynx, ρ is the air density and L is the airway length from the nasal valve to the nasopharynx. This yields friction factors, averaged over the breath cycle, of $f = 0.0028$ for the adult model and $f = 0.0145$ for the neonate model. The resistance through the neonate airway is much higher than the adult airway resistance. In addition to this, the Reynolds number is much higher for the adult. Reynolds numbers for the adult of 1760 for inspiration and 2620 for expiration agree well with those determined by Spence *et al.* [11] for the adult model. For the neonate model, Reynolds numbers of 1070 for inspiration and 670 for expiration were calculated.

There are some limitations to these models. Physiological features, such as the mucosal lining of the airways and compliance of the walls, were ignored. Wall compliance may act to reduce the local pressure and result in a decrease in the pressure difference across the airway which was not considered. The flow rate boundary conditions calculated for the neonate model were oversimplified and cannot be verified against existing data. It is possible that in the neonate model, the turbinates had further developed but the precise geometry was not captured during the segmentation process. Furthermore, the analyses performed consider natural breathing with the mouth closed, and so does not consider adults who breath predominantly through their nose. To account for natural variability between humans, different flow rates need to be investigated, and more than one geometry for the adult and neonate airway should be modelled.

Conclusions

The air flow characteristics in the nasal passages of an adult and a neonate were investigated using CFD models. Laminar flow patterns were observed in the adult model, while flow rotation in the nasal valve region of the neonate model caused large pressure drops across the airway. Higher airway resistance to flow was calculated in the neonate model. The flow patterns and velocity data from this study show good agreements with previous results obtained experimentally and numerically with similar CFD models for the adult airways. It has been difficult to compare the results for the neonate model due to the lack of data available. Further work is necessary to validate the neonate model and to compare the velocities using different flow rates.

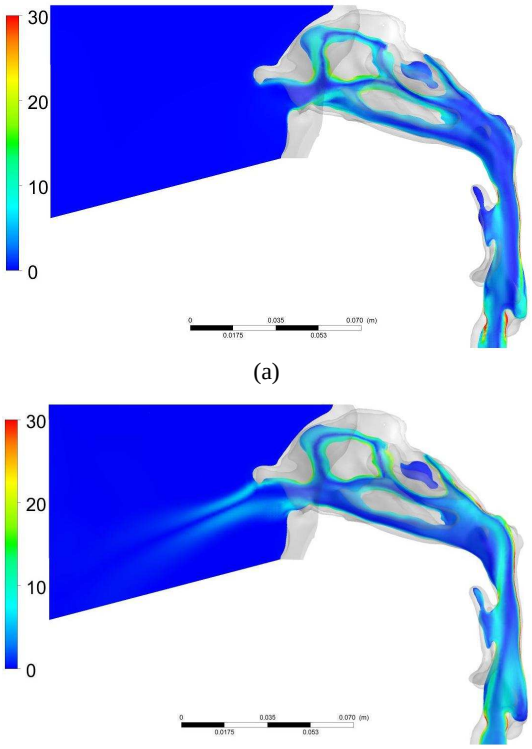

Figure 6: Profile of non-dimensional vorticity magnitude through a sagittal slice of the adult airway, during (a) inspiration and (b) expiration.

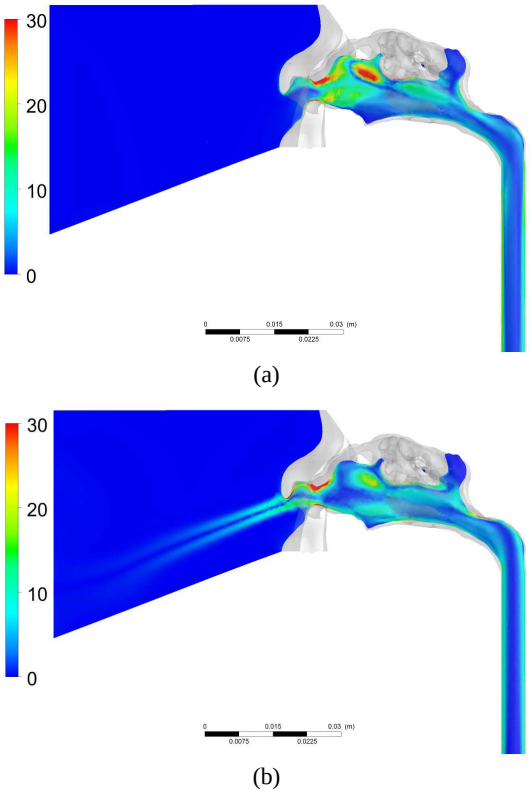

Figure 7: Profile of non-dimensional vorticity magnitude through a sagittal slice of the neonate airway, during (a) inspiration and (b) expiration.

Acknowledgements

The authors would like to acknowledge Fisher and Paykel Healthcare for supporting this undergraduate project. Also, St George's Radiology at St George's Hospital, Christchurch, New Zealand, and the Radiology Department at Auckland Hospital, New Zealand, for supplying the CT data.

References

[1] ANSYS®CFX Release 12.1, ANSYS users manual, *ANSYS Inc., Southpointe*, **275**.

[2] Croce, C., Fodil, R., Durand, M., Sbirlea-Apiou, G., Caillibotte, G., Papon, J., Blondeau, J., Coste, A., Isabey, D. and Louis, B., In vitro experiments and numerical simulations of airflow in realistic nasal airway geometry, *Annals of Biomedical Engineering*, **34**, 2006, 997–1007.

[3] Hansen, T., Cooper, T. and Weisman, L., Contemporary diagnosis and management of neonatal respiratory diseases.-, *Newtown, Pennsylvania: Handbooks in Health Care Co.*

[4] Ishikawa, S., Nakayama, T., Watanabe, M. and Matsuzawa, T., Visualization of flow resistance in physiological nasal respiration: analysis of velocity and vorticities using numerical simulation, *Archives of Otolaryngology-Head & Neck Surgery*, **132**, 2006, 1203.

[5] Janssens, H., de Jongste, J., Fokkens, W., Robben, S., Wouters, K. and Tiddens, H., The Sophia anatomical infant nose-throat (Saint) model: a valuable tool to study aerosol deposition in infants, *Journal of aerosol medicine*, **14**, 2001, 433–441.

[6] Kleinstreuer, C. and Zhang, Z., Airflow and Particle Transport in the Human Respiratory System, *Annual Review of Fluid Mechanics*, **42**, 2010, 301–334.

[7] Minocchieri, S., Burren, J., Bachmann, M., Stern, G., Wildhaber, J., Buob, S., Schindel, R., Kraemer, R., Frey, U. and Nelle, M., Development of the premature infant nose throat-model (PrINT-Model)-an upper airway replica of a premature neonate for the study of aerosol delivery, *Pediatric Research*, **64**, 2008, 141.

[8] Moody, L., Friction factors for pipe flow, *Trans. ASME*, **66**, 1944, 671–677.

[9] Mygind, N. and Dahl, R., Anatomy, physiology and function of the nasal cavities in health and disease, *Advanced Drug Delivery Reviews*, **29**, 1998, 3–12.

[10] Mylavarapu, G., Murugappan, S., Mihaescu, M., Kalra, M., Khosla, S. and Gutmark, E., Validation of computational fluid dynamics methodology used for human upper airway flow simulations, *Journal of biomechanics*, **42**, 2009, 1553–1559.

[11] Spence, C., Buchmann, N. and Jermy, M., Flow Field in the Human Nasal Cavity with Nasal High Flow Therapy from Stereoscopic PIV Measurements, in *8th International Symposium on Particle Image Velocimetry - PIV09*, Melbourne, Victoria, Australia, 2009.

[12] Taylor, D., Doorly, D. and Schroter, R., Inflow boundary profile prescription for numerical simulation of nasal airflow, *Journal of the Royal Society Interface*, **7**, 2010, 515.

[13] Tu, J., Yeoh, G. and Liu, C., *Computational fluid dynamics: a practical approach*, Butterworth Heinemann, 2008.